Measuring Time-Varying Industrial Radio Channels for D2D Communications on AGVs

Friedrich Burmeister[1], Nick Schwarzenberg[1], Tom Hößler[1,2], and Gerhard Fettweis[1,2]
[1]Vodafone Chair Mobile Communications Systems, Technische Universität Dresden, Germany
[2]Barkhausen Institut, Dresden, Germany
{friedrich.burmeister, nick.schwarzenberg, tom.hoessler, gerhard.fettweis}@tu-dresden.de

***Abstract*—Production processes coming up with Industry 4.0 will demand a high degree of flexibility since customers request more individual products. Employing wireless communication is a key enabler to meet these requirements. In order to deploy wireless systems for emerging industrial use cases in a way that both low latency as well as high reliability is guaranteed, knowledge about the radio channel is crucial. This requires representative channel measurements considering a specific use case. With this in mind, we propose a novel channel measurement approach representing industrial Device-to-Device (D2D) communication between moving Automated Guided Vehicles (AGVs), and present the obtained results. We study how obstacles affect the channel by modifying the test environment with metallic obstacles. For reproducibility, we automate the movement during the measurements using an AGV. We capture impulse responses each millisecond to resolve the time variation of the channel. It turns out that even under Non-Line-of-Sight (NLOS) conditions, the loss of receive power over the whole bandwidth is moderate due to a large number of reflections. We conclude that exploiting frequency and spatial diversity is a promising way to improve the communication reliability in industrial scenarios. We also infer that modeling the time-varying nature of channel parameters in industrial environments is feasible based on measurement data.**

***Index Terms*—Channel Measurements, Industrial, Radio Channels, Time Variation, Channel Sounding, Automated Guided Vehicle, Device-to-Device.**

I. Introduction

Next-generation assembly lines are going to be much more flexible to meet individualized production demands. Hence, automation is starting to replace cables by wireless links to cut down rearrangement and retrofitting times. Closed-loop control applications with cyclic communication pose strict requirements on latency and reliability. In [1], the 3GPP notes that the Quality of Service (QoS) of such applications is largely determined by the maximum duration of a communication outage, i.e., by the number of consecutive packet losses, instead of time-averaged metrics such as the commonly cited mean packet error rate. Therefore, it is key to understand when outages happen and how to minimize their duration. [2]

Multipath propagation and mobility of transceivers or nearby scatterers lead to radio channels that vary in frequency w.r.t. the considered system bandwidth, and in time w.r.t. the time between consecutive data packets. If we want to design and compare adaptive systems to mitigate consecutive packet errors, we need channel measurements and models that are able to reproduce the variation both in frequency and time for the targeted environment. [3] To ensure the representativeness of measurements, it is necessary to tailor the measurements to a use case of interest and consider the following aspects.

If we assume a static environment during the measurements, time variation is only caused by receiver motion with velocity $v \neq 0$, resulting in a time-varying position. The spatial measurement resolution, i.e., the distance Δx_{meas} between capture points, results from the time Δt_{meas} between capture points according to:

$$\Delta x_{\text{meas}} = v \cdot \Delta t_{\text{meas}} \tag{1}$$

If we want to study how the channel changes over time without losing information, we will have to make sure that $\Delta x_{\text{meas}} < \lambda/2$ holds, as proposed in [4], where λ corresponds to the wavelength. Measuring the channel with a mobile receiver has the advantage of capturing the Doppler effect already during the measurements. In addition to mobility, the automation of the measurement procedure is a key parameter. On one hand, automated measurements enable a very precise positioning, which is necessary if Δx_{meas} is in the order of millimeters. On the other hand, automation allows for reproducable measurements. Reproducibility will be crucial if we want to compare measurement runs for changing environments, e.g., to study the impact of obstacles. Furthermore, the elevation of the transmit and receive antennas determine whether the measurements represent a Device-to-Device (D2D) use case, i.e., both antennas have the same low elevation, or a Device-to-Infrastructure (D2I) use case, i.e., at least one antenna is mounted in a height common to an Access Point (AP) in a centralized network topology. To the best of our knowledge, we summarize existing relevant industrial channel measurements in table I to assess the contribution of our presented measurement approach. In most related works, the authors perform static channel measurements at intuitively defined positions, thereby not ensuring $\Delta x_{\text{meas}} < \lambda/2$. Those measurements do not provide information on the time-varying behavior of the channel in real applications. The authors of [5] consider a constant receiver motion in one direction during the measurements combined with a high time resolution and thus high spatial resolution. However, the covered transmission distance is still small with about $2.6\,\text{m}$ to $4.6\,\text{m}$. The authors of [6] combine channel measurements with a pick-and-place robot by attaching the receiving antenna to the gripper arm. Due to the low antenna elevation of $1\,\text{m}$ and a moving receiver antenna, a possible use case of industrial D2D communication

TABLE I: Related Work

Ref.	Autom.?	$\Delta x_{\text{meas}} < \lambda/2$?	$v \neq 0$?	D2I/ D2D?	d [m]
[7]	×	×	×	D2D	2 - 34
[8]	×	×	×	?	10 - 18
[9]	×	×	×	D2I	1 - 25
[10]	×	×	×	D2D	?
[11]	?	×	×	?	2 - 26
[12]	×	×	×	D2I	?
[13]	?	×	✓	D2D&D2I	5 - 150
[14]	×	×	✓	D2I	up to 100
[15]	×	?	✓	D2I	0 - 200
[16]	✓	✓	×	D2D	4 - 6
[6]	✓	✓	✓	D2D	1.2 - 2.7
[5]	✓	✓	✓	D2D	2.6 - 4.6
Ours	✓	✓	✓	D2D	1 - 10

is addressed. Furthermore, the authors are able to measure the channel continuously, i.e., with minimum distance between the capture points. However, the gripper arm can only move within a certain radius, which also limits the covered transmission distances of the measurement.

In this paper, we present a novel channel measurement approach and results for D2D communications in industrial environments. By attaching measurement hardware to an Automated Guided Vehicle (AGV) during the measurements, we not only address a new industrial use case for D2D communication, but also cover larger and thus more representative transmission distances than existing measurements. In addition, the AGV enables taking high receiver mobility into account as well as the implementation of a highly automated and therefore reproducible measurement procedure. A further novelty of our measurement campaign is a flexible test environment, that we modify with help of metallic reflectors to create Line of Sight (LOS) and Non-Line-of-Sight (NLOS) conditions. Thus, in combination with measurement automation, we study the impact of obstacles in industrial environments with respect to receive power, delay spread and coherence bandwidth.

The remainder of this paper is organized as follows: In section II, the measurement components and methodology are described. Section III introduces the necessary data processing steps. In section IV, we present results observed from the measurement data. A conclusion is drawn in section V.

II. Measurements

A real application with D2D communication between AGVs would allow that both communication participants are in motion. For the sake of reproducibility, we choose to keep the transmitter position static and only move the receiver. For the same reason, we choose not to include randomness, e.g., by walking persons. We attach measurement hardware to an AGV to measure the radio channel. The environment is modified by additional obstacles to create LOS and NLOS conditions. A brief description of the individual components follows.

Fig. 1: The size of the surrounding area in which the measurement environment is integrated is about $12\,\mathrm{m} \times 22\,\mathrm{m}$. The available test area itself has a size of $11\,\mathrm{m} \times 8\,\mathrm{m}$.

A. Measurement Area

Specific test environments cause significant deviations in the results of industrial radio channel measurements [17]. One reason is the great variety of industrial environments. The area selected for our measurements is located in a industrial hall. Since it is a test site, there is no permanent installation such as big machines. The propagation characteristics are dominated by the surrounding walls and metal structures, e.g., cable and pipe ducts, supporting and load-bearing metal beams near the ceiling. There is also a reflecting and diffusing truss construction surrounding the test area (see Fig. 1). The ceiling height is $7.6\,\mathrm{m}$ and the floor is covered with linoleum. Thus, the channel conditions are not too special and allow for generalization towards similar environments. We modify its characteristics in terms of reflections and shadowed areas by placing metallic walls of $2\,\mathrm{m}$ height.

B. AGV for Receiver Mobility

Fig. 2a shows the AGV with the measurement hardware on top. The velocity of the AGV can be configured up to a maximum of $1\,\mathrm{m/s}$. In order to observe the worst-case Doppler shift, and to perform the measurements as fast as possible, we select $1\,\mathrm{m/s}$. Besides the velocity, the trajectory of the AGV is configurable. We prepare a wide course, resulting in a recording duration of $20\,\mathrm{s}$. The key benefit of using an AGV for emulating a mobile receiver is the uniformity and reproducibility of its motion. This behavior allows us to compare different measurement rounds, even when the test environments changes, and, thus, study the impact of metallic obstacles on the radio channel. The antenna on the AGV has an elevation of $80\,\mathrm{cm}$. We place the stationary transmitter antenna at the same height as the receiver antenna (see Fig. 2b) to represent the D2D use case.

C. Creating Scenarios with Reflectors

The empty measurement environment, as shown in Fig. 1, already provides a certain reflectivity and characteristic footprint with respect to the radio channel. However, real production plants contain obstacles, e.g., machines and robots. These cause areas where the LOS between AGV and AP or between two AGVs is lost. Using freely arrangeable metal

(a) Measurement hardware attached to a moving AGV.

(b) Stationary transmitter placed next to the test area.

Fig. 2: The transmit and receive antennas are elevated to a height of 80 cm to represent a D2D link.

Fig. 3: The test site is modified by placing metal walls to create LOS and NLOS areas. The AGV moves around both obstacles. Figure 4a shows the corresponding map of this scenario.

walls as shown in Fig. 3, we can intuitively create a variety of scenarios to investigate the effects of obstacles on the channel. The entire measurement campaign includes the construction of 10 scenarios in total. For each scenario, we capture 10 repetitions, i.e., 10 rounds.[1]

Fig. 4 shows maps of two created scenarios, which we refer to as "machines scenario" and "wall scenario". We refer to the case without obstacles as "empty scenario". The route of the AGV is marked in green and the position of the obstacles in red. Black points indicate the time-dependent position of the AGV. Depending on the obstacle placement, the vehicle experiences both LOS and NLOS conditions, and the transitions between them. Besides, there are packages of metallic content on the test surface as indicated on the map.

[1]Within these 10 scenarios, two AGV trajectories were considered. In addition to the presented horizontal route, we used a vertical route in the left half of the area. Scenarios not presented in this work but included in the data set cover different distances between the AGV and the obstacles as well as paths between obstacles, e.g., when the AGV passes a corridor of varying widths. The measurement data of all scenarios will be gladly provided upon request.

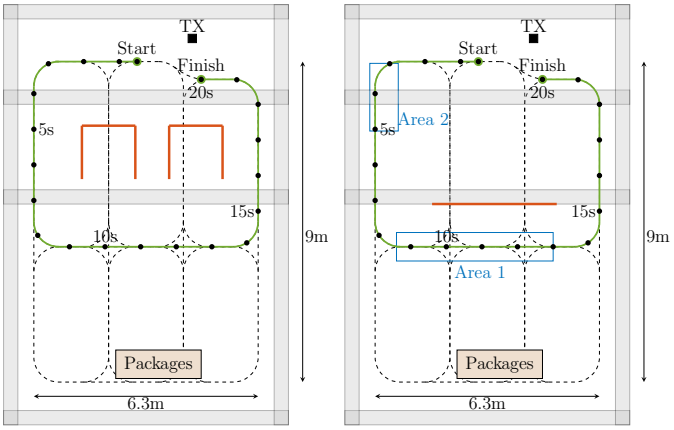

(a) Machines Scenario (b) Wall Scenario

Fig. 4: The maps show a selection of constructed measurement scenarios. The empty scenario uses the same track, but without metal walls. The AGV route is marked in green, overlayed by black dots indicating the AGV position at whole seconds. The red lines indicate the positions of the metal walls. Areas 1 and 2 are used to quantify the delay spread and the frequency selectivity in section IV-D.

D. Hardware Configuration

We focus on the frequency band from 3.7 GHz to 3.8 GHz, because it has been recently made available in Germany for local industrial communications [18] and is adjacent to the global 5G band 48. The measurement hardware consists of two NI Universal Software Radio Peripheral (USRP) 2974 as transmitter and receiver, respectively. To avoid distortions caused by the amplifier, we set the transmission power to 10 dBm. The transmit antenna is a wideband monopole antenna with a flat structure. An omni-directional vertical antenna is used on the receiver side. Table II gives an overview of the measurement parameters.

E. Measurement Methodology

Measuring time-varying mobile radio channels in real-time requires efficient methods. The traditional way of measuring a channel using frequency sweeps is not advisable, as the sweep duration limits the measurement interval Δt_{meas}. Instead, we transmit a known signal over the entire bandwidth and obtain the instantaneous channel response by correlation. We choose Zadoff-Chu (ZC) sequences with a length of $N_{\text{ZC}} = 512$ samples and a displacement parameter $m = 1$ as periodic sounding signal because of their favorable correlation properties [19]. At the start of each measurement round, the receiver is triggered by the AGV's acceleration using a gyro sensor and starts to capture snapshots of 100 µs duration periodically. As the obtained data should support accurate link-level modeling and simulations, the measurement interval Δt_{meas} should be in the range of the transmission intervals of modern wireless systems, i.e., in the order of 1–10 ms [1]. Therefore, we set Δt_{meas} to 1 ms. For a velocity of 1 m/s, this corresponds to $\Delta x_{\text{meas}} = 1\,\text{mm}$ according to Eq. 1. To justify the time between capture points with respect to the coherence time of the channel, we compared channel responses

TABLE II: Measurement Parameters

Carrier Frequency	3.75 GHz	RX Bandwidth	100 MHz
Sampling Period	10 ns	Length ZC sequence	512 samples
Δt_{meas}	1 ms	Snapshot Duration	100 µs
AGV Velocity	1 m/s	AGV Track Length	18 s to 20 s
TX Distance	1–10 m	TX Power	10 dBm
Antenna Config.	SISO	Antenna Elevation	0.8 m

from consecutive snapshots for worst-case NLOS conditions and observed that the changes between them were smooth. In addition, we carried out measurements with higher temporal resolution and found that extra snapshots in between did not reveal additional detail. Furthermore, [4] defines Δt_{meas} as sufficient if it satisfies the condition

$$\Delta t_{\text{meas}} \leq \frac{c_0}{2 f_c v_{\text{max}}} = 40\,\text{ms} \tag{2}$$

which confirms our empirical findings. We conclude that a measurement interval of 1 ms is more than sufficient for the considered velocity. To ensure that the desired Δt_{meas} is met, we make use of the Field Programmable Gate Arrays (FPGAs) on the USRPs. A clock-driven LabVIEW application maps the timestamp of each measurement snapshot to a location in the test area.

III. Data Processing

Since a real system suffers from hardware imperfections, we have to compensate them. The first processing step consists of correcting the DC offset in the received signal. The channel impulse responses (CIRs) are computed from the captured snapshots by cross-correlation with the chosen ZC sequence [4]. A snapshot of 100 µs contains 18 ZC sequences, leading to 18 CIRs after cross-correlating. The Carrier Frequency Offset (CFO) caused by mismatching local oscillators of transmitter and receiver and by the Doppler effect is estimated and corrected according to the time offset and phase of these periodic CIRs. Besides the CFO, a Sampling Frequency Offset (SFO) occurs due to the lack of synchronization between the transmitter's and receiver's sampling clock. For noise suppression, the CFO-corrected CIRs can be averaged, assuming that the channel does not change within the duration of a snapshot [4]. As the snapshot duration is only a fraction of the measurement interval (see section II-E), this assumption seems legitimate. The final step in preparing the data involves an energy normalization of each impulse response $h(t)$ according to

$$\tilde{h}(t) = \frac{h(t)}{\sqrt{\sum_k h^2(t, \tau_k)}} \tag{3}$$

where $\tilde{h}(t)$ is the energy-normalized CIR and the index k corresponds to the k-th tap with delay τ_k in the CIR at time t. This step is necessary to get similar scales when we compare CIRs under both LOS and NLOS conditions later on.

IV. Results

This section presents findings based on the measurements. In general, the investigations refer to the time variation of the radio channel.

A. Channel Impulse Responses

First, we take a look at exemplary CIRs to qualitatively assess the time variation of the radio channel. Fig. 5 shows CIRs over a period of 50 ms which were captured in both LOS and NLOS areas, exemplary at 18 s and 9 s in the machines scenario (see Fig. 4a). At this point, we would like to illustrate the relation between time variation and coherence time. The coherence time itself, i.e., the time in which the CIR can be assumed to remain constant, is a time-variant quantity on a larger time scale. Fig. 5 underlines this observation. Depending on the position of the AGV and the associated LOS condition, the coherence time differs – it varies over time. The coherence time is connected to the change of the CIR. In the LOS range, the CIRs are characterized by a slowly changing, dominant LOS path. However, in the NLOS area, they are composed of many multipath components of similar power, without a dominant LOS component. At the same time, the paths are subject to stronger variations in the same considered time span, i.e., the channel changes faster.

B. Channel Frequency Responses

Complementing the time-domain CIRs, we want to discuss the frequency responses of the channel at the selected points in time.. Fig. 6 shows the power density spectra corresponding to the CIRs illustrated in Fig. 5, i.e., for LOS and NLOS, respectively. Comparing the spectra on the same scale reveals a higher average channel gain under LOS conditions, caused by the LOS component and a lower transmission distance. However, the comparison with respect to fading depth is more interesting. The exemplary LOS spectrum shows no fading dips deeper than 5 dB, i.e., there are no deep fades. Under NLOS conditions, destructive interference happens more often due to superposition of multiple NLOS paths and the fact that there are many incoming paths with similar power. Therefore, we expect stronger fading in the spectrum. The corresponding spectrum in Fig. 6b indicates deeper fades with drops of up to 14 dB, indicating a more frequency-selective channel. The coherence bandwidths presented in section IV-D underline this observation.

What does this mean for a communication system in practice? Assuming that the investigated frequency range is divided into sub-channels, some of these channels may suffer from significant distortion while other channels experience only minor attenuation. Especially under NLOS conditions, we conclude that exploiting frequency diversity is promising in order to improve the communication reliability in industrial environments.

C. Receive Power

With a high time resolution, we can demonstrate the temporal variability of the channel caused by the AGV's motion.

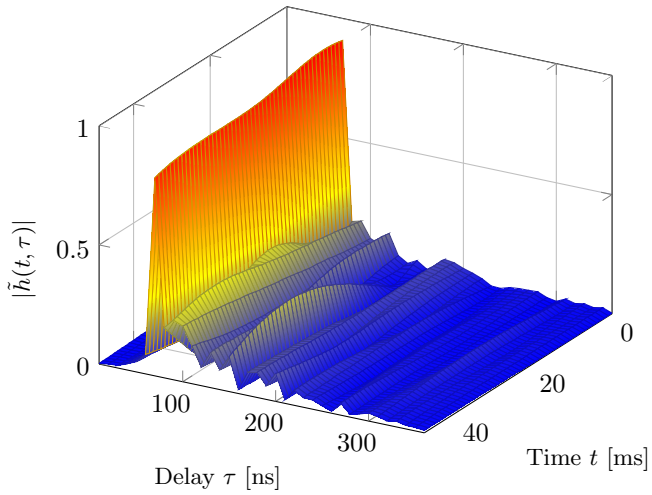

(a) Consecutive CIRs under LOS conditions show a strong and slowly changing dominant path.

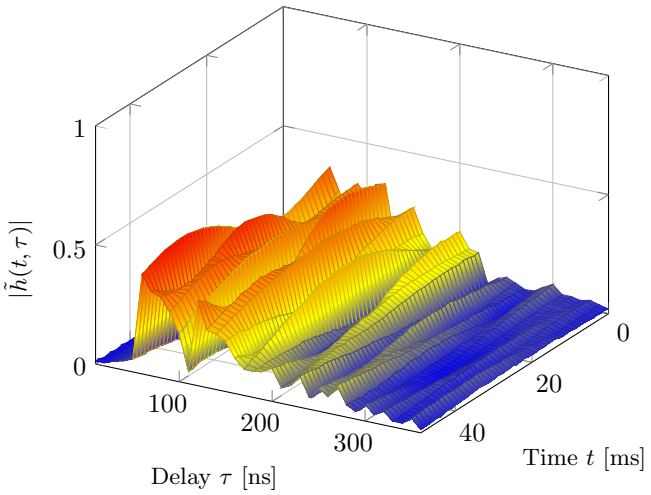

(b) Consecutive CIRs under NLOS conditions, e.g., behind obstacles, show a multitude of rapid varying channel components.

Fig. 5: Energy-normalized CIRs captured with a rate of 1 kHz show that the time variability differs according to the LOS conditions.

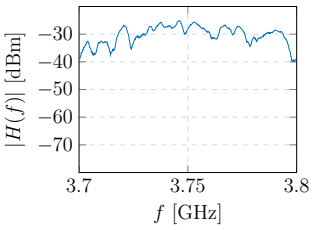

(a) There are no deep fades in the spectrum corresponding to Fig. 5a.

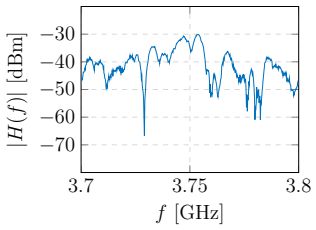

(b) The spectrum corresponding to Fig. 5b shows more severe attenuation caused by fading.

Fig. 6: Comparison of a LOS and a NLOS spectrum.

Fig. 7 shows the total receive power P_{Rx} over the whole measurement bandwidth for the scenarios shown in Fig. 4. The relation between transmission distance and receive power is clearly visible. At the same time, we can see similarities and deviations between different scenarios. The receive power graph without obstacles, i.e., for the empty scenario, serves as a baseline. This is the inherent channel footprint that the factory environment provides. Local interference causes characteristic features to appear throughout the course. For example, after about 6 s the AGV is near a metal beam. The transmit antenna, the AGV and the metal beam are on one line, resulting in constructive interference and hence an increased receive power. Note that these interference patterns match for different scenarios. For the machines scenario (see Fig. 4a), the LOS is blocked at this point, which leads to decreased power compared to the other scenarios. Nevertheless, a power gain is still noticeable due to the reflection of NLOS components at the metal beam. In the window from 6 s to 14 s, we can observe shadowing caused by obstacles. Considering the map of the wall scenario in Fig. 4b, one can estimate the beginning of the NLOS section after about 8.5 s by visually determining the obstructed area. This estimation is reinforced by assessing the power trend since the curves separate at this point. The end of the NLOS area behaves analogously after 13 s for the wall scenario. From 8.5 s to 13 s, the average receive power behind the wall is about 3.5 dB lower compared to the empty test area. With 8 dB, the largest attenuation caused by the wall occurs after 11 s, where the wall prevents the occurrence of a constructive interference. Taking a look at the machines scenario, we can see a characteristic LOS window from 10 s to 11 s which corresponds to the free space between the two machines. Apart from expected power degradation in NLOS areas, we would like to draw attention to power increasing effects due to obstacles. This happens in front of the obstacles when they provide strong reflections. The receive power evaluations show that the power loss caused by obstacles is only about 3.5 dB on average. This observation is plausible due to the high environmental reflectivity and the relatively large receive bandwidth. We expect that in practice, changing from LOS to NLOS conditions is not critical in terms of receive power for high-bandwidth wireless systems since the decrease does not exceed common fade margins.

Besides, evaluating the receive power in narrower sub-channels is also important, since state-of-the-art cellular and Wi-Fi systems may use only a portion of the available band. That is why we compare the time-variant receive power of two non-adjacent 10 MHz sub-channels, considering the time range from 6 s to 14 s of the machines scenario. The receive power of a sub-channel is computed from the frequency response by integrating over the frequency range of the respective channel. According to Fig. 8, we observe that the time variation is different for the investigated sub-channels. Since various frequency ranges are affected by different multipath components, there are individual points of interference per channel. In contrast to the full bandwidth, the drops of receive power coming with the position changes are more significant with up to 15 dB.

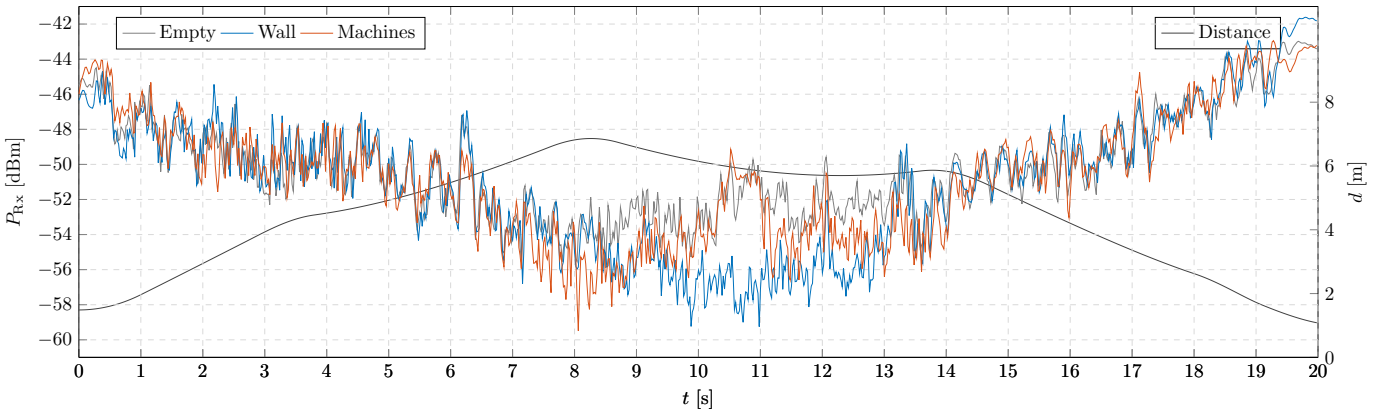

Fig. 7: Thanks to our highly automated measurement setup, we can compare the receive power from three different measurement scenarios for a whole round. A detailed look at the graphs reveals a good match between the scenarios, with deviations caused by obstacles. For instance, environment-specific points of constructive interference at $t = 6.2\,\mathrm{s}$ and $t = 12\,\mathrm{s}$ become visible in all scenarios. Depending on the obstacles, these features are attenuated, but still present.

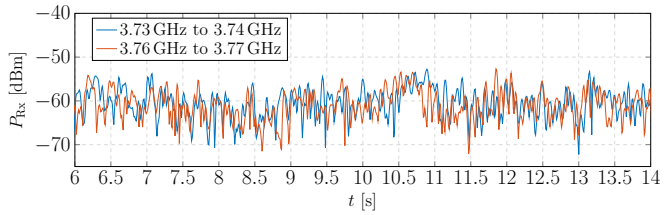

Fig. 8: Considering the receive power of 10 MHz sub-channels instead of the complete measurement bandwidth, we see more severe power drops depending on the time-varying position of the receiver. Also, the distinctive interference patterns do not match for different sub-channels.

D. Channel Parameters

In order to quantify the delay spread and the frequency-selectivity of the channel, and to investigate the impact of metallic obstacles, we determine the channel parameters root mean square delay spread τ_{rms} and coherence bandwidth B_{coh} for the exemplarily chosen areas indicated in Fig. 4b.

τ_{rms} is computed according to [20]

$$\tau_{\mathrm{rms}} = \sqrt{\frac{\sum_k P_{\mathrm{Rx}}(\tau_k)\tau_k^2}{\sum_k P_{\mathrm{Rx}}(\tau_k)} - \left(\frac{\sum_k P_{\mathrm{Rx}}(\tau_k)\tau_k}{\sum_k P_{\mathrm{Rx}}(\tau_k)}\right)^2} \tag{4}$$

where τ_k and $P_{\mathrm{Rx}}(\tau_k)$ are the delay and power of the k-th channel tap, respectively. Beforehand, we have to extract the relevant taps that belong to the CIR. We use an iterative approach similar to the one presented in [21] and ensure that the power of the first channel tap is no lower than 20 dB below the largest channel component.

The coherence bandwidth B_{coh} is computed according to [4] based on the channel frequency response.

Table III contains the empirical mean μ and standard deviation σ as well as minimum and maximum values for each channel parameter, scenario and selected area. By evaluating these measures for the empty and the wall scenario, we are able to quantify the impact of metallic obstacles. Area 1 is located such that the wall scenario causes NLOS conditions.

TABLE III: Selected Measurement Results

Area	Scen.	τ_{rms} [ns]				B_{coh} [MHz]			
		μ	σ	min	max	μ	σ	min	max
1	Empty	52.2	6.2	34.4	71.5	11.5	7.0	3.4	39.7
	Wall	59.7	6.5	40.5	87.3	5.8	4.4	2.4	33.5
2	Empty	45.4	5.3	29.4	59.9	16.8	9.1	4.0	38.7
	Wall	42.9	5.8	25.4	57.0	16.3	8.2	4.0	42.4

Both the mean as well as the maximum B_{coh} are about 6 MHz lower due to the wall. As expected, the τ_{rms} increases when the wall blocks the LOS.

In area 2 however, there are LOS conditions in both of the scenarios. The mean coherence bandwidth is of similar order of magnitude, but the maximum B_{coh} is about 4 MHz higher in the wall scenario. We also want to highlight that the mean τ_{rms} is smaller in area 2 when the metal wall is placed. We explain this observation by the positive effect of obstacles due to the blockage of far reflections if the LOS exists.

The selected areas represent only a part of the measured distances. By plotting τ_{rms} over the distance d (see Fig. 9a), we see the correlation of these parameters for the empty scenario. Since the receive power P_{Rx} is also correlated with d, as shown in Fig. 9b, we expect a correlation between τ_{rms} and P_{Rx}. Fig. 9c confirms the expected negative correlation. Besides internally validating our measurements, the correlation plots draw attention to the remarkably increasing delay spread, which is normally seen in NLOS and outdoor conditions. The authors of [6] evaluate τ_{rms} for distances of 1 m to 3 m and present a similar dependence. Our results confirm that the correlation holds for larger distances as well.

V. Conclusion

In this work, we proposed a novel method for measuring time-varying radio channels in industrial environments. We conducted a measurement campaign using said method and evaluated selected results. By employing an AGV to emulate

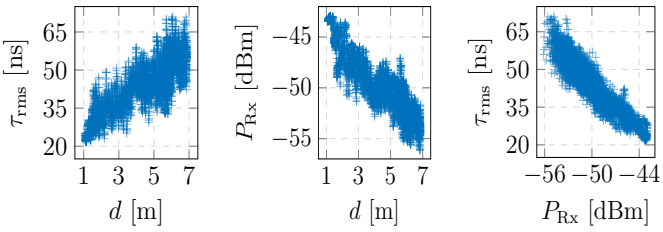

(a) Delay spread vs. distance

(b) Receive power vs. distance

(c) Delay spread vs. receive power

Fig. 9: Considering the empty scenario, correlations between P_{Rx}, τ_{rms} and d are visible. Not only the power decreases with increasing distance, but also τ_{rms} increases with distance, even under LOS conditions. We observe a negative correlation between τ_{rms} and P_{Rx}.

a mobile receiver in a reproducible way, combined with a low antenna elevation, we were able to model an industrial D2D use case. It turns out that the drop of combined wideband receive power in NLOS areas is less severe than in other environments due to the multitude of good reflectors along the propagation path. We conclude that exploiting frequency and spatial diversity is promising in order to increase the communication reliability in industrial environments with high reflectivity. Thanks to the reproducibility of the measurements, we showed that the environment causes a characteristic channel footprint with respect to positions of constructive and destructive interference. This raises the question of how industrial radio channels can be modeled properly, since it is crucial to consider its time-variant behavior if we want to investigate the communication reliability. Deterministic models, including ray tracing approaches, would require high-resolution 3D models of the environment. In addition, the assumption of static environments does not hold in real industrial scenarios. To overcome these challenges, a measurement-based modeling approach seems more appropriate. That is why we are currently developing a channel model which is able to represent the time-varying behavior of the radio channel and is parameterized using quick measurements like the ones we presented in this work.

In order to give other researchers the opportunity to reproduce the presented results and to pursue further analysis, we make the measurement data freely accessible. We will gladly provide the raw measurement data and our MATLAB scripts for CIR computation upon request.

Acknowledgment

This work was supported by the German Federal Ministry of Education and Research (BMBF) as part of the project "TACNET 4.0" under grant 16KIS0719 and as part of the project "AI4Mobile" under grant 16KIS1177. This research was co-financed by public funding of the state of Saxony/Germany. The authors would like to thank Dr. Monique Düngen and Thomas Hansen from Robert Bosch GmbH for many fruitful discussions and providing the test site, and Götting KG for providing their "KATE" AGV.

References

[1] 3GPP, "Service requirements for the 5G system (Rel. 17)," 3rd Generation Partnership Project (3GPP), Technical Specification (TS) 22.261, Dec. 2019, version 17.1.0.

[2] T. Hößler, P. Schulz, M. Simsek, and G. P. Fettweis, "Mission Availability for Wireless URLLC," in *IEEE Global Communications Conference (GLOBECOM)*, 2019.

[3] H. Tataria, M. Shafi, A. Molisch, M. Dohler, H. Sjöland, and F. Tufvesson, "6G Wireless Systems: Vision, Requirements, Challenges, Insights, and Opportunities," *Proceedings of the IEEE*, Aug. 2020, invited Article in the Proceedings of the IEEE.

[4] A. F. Molisch, *Wireless Communications, 2nd Edition*. Wiley-IEEE Press, 2010.

[5] S. Zelenbaba, M. Hofer, D. Löschenbrand, G. Kail, M. Schiefer, and T. Zemen, "Spatial Properties of Industrial Wireless Ultra-Reliable Low-Latency Communication MIMO Links," in *53rd Asilomar Conference on Signals, Systems, and Computers*, 2019.

[6] B. Holfeld, D. Wieruch, L. Raschkowski, T. Wirth, C. Pallasch, W. Herfs, and C. Brecher, "Radio channel characterization at 5.85 GHz for wireless M2M communication of industrial robots," in *IEEE Wireless Communications and Networking Conference*, 2016.

[7] D. A. Wassie, I. Rodriguez, G. Berardinelli, F. M. L. Tavares, T. B. Sorensen, and P. Mogensen, "Radio Propagation Analysis of Industrial Scenarios within the Context of Ultra-Reliable Communication," in *IEEE 87th Vehicular Technology Conference (VTC Spring)*, 2018.

[8] Y. Ai, M. Cheffena, and Q. Li, "Power delay profile analysis and modeling of industrial indoor channels," in *9th European Conference on Antennas and Propagation (EuCAP)*, 2015.

[9] Z. Irahhauten, G. J. M. Janssen, H. Nikookar, A. Yarovoy, and L. P. Ligthart, "UWB channel measurements and results for office and industrial environments," in *IEEE International Conference on Ultra-Wideband*, 2006.

[10] E. I. Adegoke, R. M. Edwards, W. G. Whittow, and A. Bindel, "Characterizing the Indoor Industrial Channel at 3.5 GHz for 5G," in *Wireless Days (WD)*, 2019.

[11] J. Narrainen and R. D'Errico, "Large Scale Channel Parameters in Industrial Environment," in *13th European Conference on Antennas and Propagation (EuCAP)*, 2019.

[12] M. Schmieder, T. Eichler, S. Wittig, M. Peter, and W. Keusgen, "Measurement and Characterization of an Indoor Industrial Environment at 3.7 and 28 GHz," in *14th European Conference on Antennas and Propagation (EuCAP)*, 2020.

[13] S. Jaeckel, N. Turay, L. Raschkowski, L. Thiele, R. Vuohtoniemi, M. Sonkki, V. Hovinen, F. Burkhardt, P. Karunakaran, and T. Heyn, "Industrial Indoor Measurements from 2-6 GHz for the 3GPP-NR and QuaDRiGa Channel Model," in *IEEE 90th Vehicular Technology Conference*, 2019.

[14] Z. Kun, L. Liu, T. Cheng, Y. Ze, and Z. Jianhua, "Channel Measurement and Characterization for Industrial Internet of Things," in *IEEE Wireless Communications and Networking Conference (WCNC)*, 2019.

[15] R. Candell, C. A. Remley, J. T. Quimby, D. R. Novotny, A. Curtin, and P. B. Papazian, "Industrial wireless systems: Radio propagation measurements," National Institute of Standards and Technology (NIST), Technical Report, 2017.

[16] W. Debaenst, A. Feys, I. Cuiñas, M. Sánchez, and J. Verhaevert, "RMS Delay Spread vs. Coherence Bandwidth from 5G Indoor Radio Channel Measurements at 3.5 GHz Band," *Sensors 2020*, vol. 20, 01 2020.

[17] J. Ferrer Coll, P. Ängskog, J. Chilo, and P. Stenumgaard, "Characterisation of highly absorbent and highly reflective radio wave propagation environments in industrial applications," *Communications, IET*, vol. 6, Oct. 2012.

[18] "Frequenzzuteilungen für lokale Frequenznutzungen im Frequenzbereich 3,700-3,800 MHz," Bundesnetzagentur für Elektrizität, Gas, Telekommunikation, Post und Eisenbahnen, Verwaltungsvorschrift, Nov. 2019.

[19] R. Frank, "Polyphase codes with good nonperiodic correlation properties," *IEEE Transactions on Information Theory*, vol. 9, no. 1, 1963.

[20] T. S. Rappaport, *Wireless Communications, Principles and Practice*. Prentice Hall, 2002.

[21] S. Jaeckel and V. Jungnickel, "Estimating MIMO capacities from broadband measurements in a cellular network," in *Proceedings of the Fourth European Conference on Antennas and Propagation*, 2010.